STRUCTURAL CONTROL AND HEALTH MONITORING
Struct. Control Health Monit. 2008; **15**:673–696
Published online in Wiley InterScience
(www.interscience.wiley.com). DOI: 10.1002/stc.269

Semiactive control strategy for a phase II smart base isolated benchmark building

Chia-Ming Chang[1], Kyu-Sik Park[2,‡], Alan Mullenix[1] and Billie F. Spencer Jr[1,*,†]

[1]*Department of Civil and Environmental Engineering, University of Illinois at Urbana-Champaign, Urbana, IL 61801, U.S.A.*
[2]*Steel Structure Research Laboratory, Research Institute of Industrial Science and Technology (RIST), 79-5 Yeongcheon, Dongtan, Hwaseong, Gyeonggi-do 445-813, Korea*

SUMMARY

This paper presents a semiactive control strategy for the seismic protection of the phase II smart base isolated benchmark building subjected to near-fault earthquakes. Magnetorheological (MR) fluid dampers controlled by an optimal direct output feedback control algorithm with a voltage generator are used as semiactive control devices. The benchmark building is an eight-story base isolated building, and the superstructure is considered to be a linear elastic system with lateral–torsional behavior. To reduce the energy transmitted to the structure from the ground, a combination of linear and nonlinear bearings is installed at the base of the structure. It is difficult to design the controller for this benchmark problem because of the nonlinear behavior of the isolation members. Linear control theory is frequently applied to nonlinear structures because there are no appropriate and well-defined control theories that can consider general types of nonlinearities. Therefore, to improve control performance, the nonlinearities of the isolation members are considered indirectly with the linear control theory during the design process of the controllers for the MR dampers. Numerical simulation results under various earthquake inputs show that the proposed control strategy is effective in reducing the responses of the isolation members as well as the superstructure. Therefore, the proposed control system could be used as an improved control strategy for base isolated buildings subjected to near-fault earthquakes. Copyright © 2008 John Wiley & Sons, Ltd.

KEY WORDS: benchmark isolated building; magnetorheological fluid damper; direct output feedback control; seismic response control; simplified nonlinear control strategies

*Correspondence to: Billie F. Spencer Jr, Department of Civil and Environmental Engineering, University of Illinois at Urbana-Champaign, Urbana, IL 61801, U.S.A.
†E-mail: bfs@uiuc.edu
‡Senior researcher.

Contract/grant sponsor: National Science Council in Taiwan; contract/grant number: NSC-095-SAF-I-564-036-TMS
Contract/grant sponsor: National Science Foundation; contract/grant number: 06004330301140

Received 19 May 2007
Revised 1 April 2008
Accepted 8 April 2008

1. INTRODUCTION

Many control strategies have been proposed and implemented over the last few of decades for the purpose of protecting structures against natural hazards such as severe earthquakes and strong winds. One of the most widely implemented and accepted control strategies is seismic isolation systems [1,2]. Essentially, this technique consists of the installation of mechanisms that decouple the structure and its components from potentially damaging earthquake-induced ground or support motions. The phase II smart base isolated benchmark building also uses a combination of linear and nonlinear bearings to protect the building from near-fault earthquakes. In base isolation systems, nonlinear devices such as lead rubber bearings (LRBs), friction pendulum and high-damping rubber bearings are often used. The main advantage of these types of bearings is that a restoring force and an adequate damping capacity can be obtained in one device. However, because the dynamic characteristics of these bearings are highly nonlinear, the vibration reduction of the bearings is not optimal for a wide range of input ground motion intensities, particularly strong impulsive ground motions generated at near-source locations [3,4]. Furthermore, these seismic isolation systems allow large deformations of the bearings to shift the natural frequency of the structure away from the frequency range in which the earthquake energy is concentrated. These large deformations in the isolated structure could cause many critical problems such as excessive drift in buildings and collapse as well as pounding of decks in bridges. Therefore, recent revisions to the Uniform Building Code [4] mandate the accommodation of larger base displacements and the consideration of a stronger maximum credible earthquake, indirectly suggesting the need for supplemental damping devices [5]. To address the limitations of passive-type seismic isolation systems, an improved control strategy combined with semiactive and/or active control devices can be used. This system could alleviate some of the restrictions and limitations that exist when each system is acting independently.

In this study, magnetorheological (MR) dampers are used as semiactive control devices and an optimal direct output feedback control algorithm is used as the primary control scheme to calculate the required control force for the MR dampers. Moerder and Calise [6] proposed optimal output feedback control while considering convergence of the algorithm. As an alternative, direct output feedback control, which neglects the design of the Kalman, has been proposed by some researchers [7,8]. The secondary control scheme generates the command voltage to the MR fluid dampers based on an inverse dynamic model of the MR dampers. During the controller design, two different nonlinear models for the frictional pendulum bearings are considered. First, a simple bilinear model that can capture the main characteristics of the friction pendulum bearings is used. Four different controllers are designed based on the pre- and post-yield stiffness of the friction pendulum in both the x- and y-direction. Depending on the current status of the friction pendulum, one of the four controllers will be applied at any given time step during an earthquake event. The model provided in the problem definition paper [9] is used as the second model of the frictional pendulum. The re-centering stiffness of the frictional pendulum is used to obtain the linear model of the benchmark structure, and this linear model is used during the controller design. However, the compensated force coming from the nonlinear terms of the frictional bearings is added to the optimal control force.

Following a summary of the benchmark problem statement, a control strategy using semiactive devices and the results of numerical simulations under various earthquake excitations are presented to demonstrate the efficacy of the proposed control strategy.

DOI: 10.1002/stc

2. A BRIEF SUMMARY OF THE BENCHMARK PROBLEM

In this section, a brief review of the phase II smart base isolated benchmark building is given. A detailed description of the benchmark control problem for the base isolated building including the mathematical model, input excitations, evaluation criteria and three-dimensional nonlinear dynamic analysis program using MATLAB® [10] can be found in the problem definition paper [9]. For the linear base isolated structure, many researchers have proposed different control strategies and have reported their results in the earlier published special issue of the phase I smart base isolated benchmark problem [11]. For the nonlinear cases in the benchmark problem, some control strategies have been proposed considering bilinear and nonlinear hysteretic models for the isolation system [12,13].

The benchmark structure is a base isolated eight-story, steel-braced framed building that is 82.4-m long and 54.3-m wide as shown in Figure 1.

The superstructure is modeled as a three-dimensional linear elastic system using three degrees of freedom (DOF) per floor at the center of mass so that the superstructure consists of 24 DOFs. All 24 modes in the fixed-base structure are used in modeling the superstructure, and the damping ratio is assumed to be 5% in all fixed-base modes. The computed first natural periods

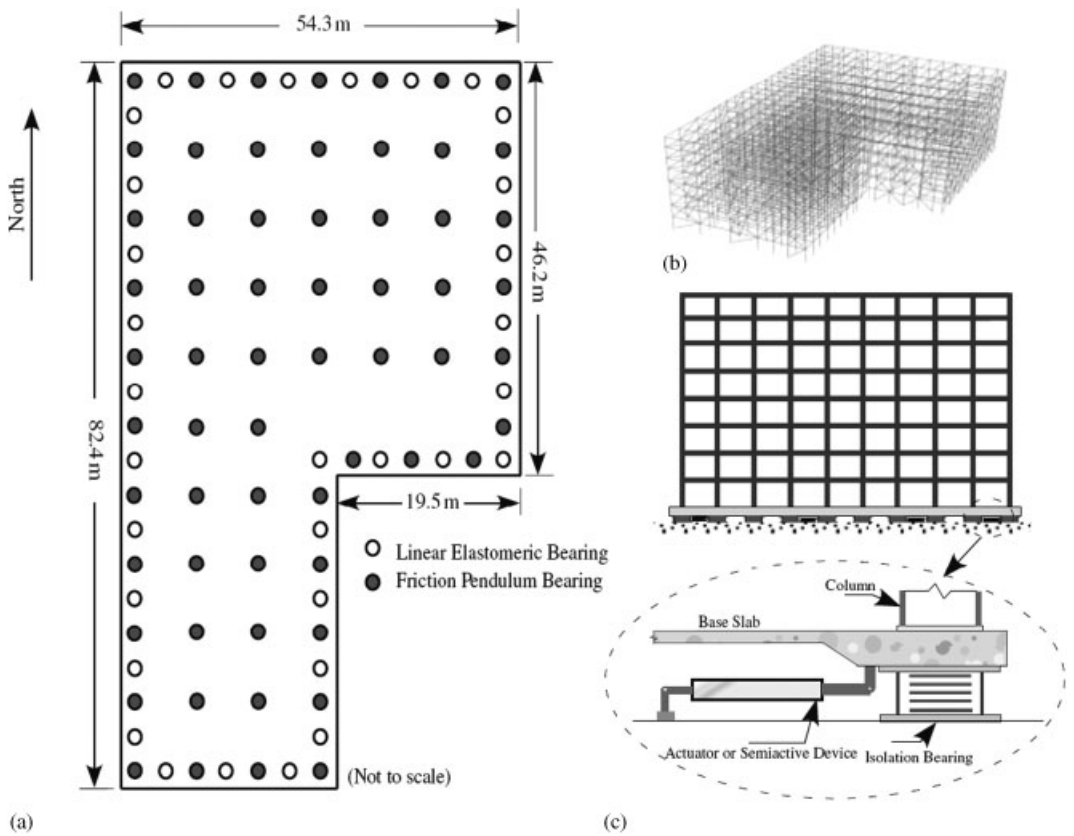

Figure 1. Phase II smart base isolated benchmark building [9].

DOI: 10.1002/stc

of the fixed-base modes are 0.78, 0.89 and 0.15 s in the North–South, East–West directions and in torsion, respectively. The base is also modeled with three DOFs located at the center of mass of the base so that the whole base isolated benchmark building consists of 27 DOFs.

To decouple the structure from potentially damaging earthquake-induced ground or support motions and to enhance the structural safety, 61 nonlinear isolation bearings (i.e. friction pendulum or LRBs) and 31 linear elastomeric bearings are installed at the base of structure as shown in Figure 1. These isolation devices are elastic, viscous, hysteretic elements for bilinear LRBs and hysteretic elements for the friction pendulum bearings. The biaxial hysteretic behavior of LRBs and frictional bearings is modeled using the biaxial interaction equation of the Bouc–Wen model [14]. In addition, a total of 16 MR dampers are also installed with the isolation system for the semiactive system. The resultant control force from the isolator and the additional control devices are transferred to the center of mass of the base and may cause rotational effects.

To evaluate the effectiveness of the control system, evaluation criteria, J_1–J_9, have been presented in the problem definition paper [9]. The first five evaluation criteria, J_1–J_5, are related to the peak responses, where J_1 = peak base shear, J_2 = peak structure shear, J_3 = peak base displacement, J_4 = peak interstory drift and J_5 = peak floor acceleration. These evaluation criteria are normalized with respect to the uncontrolled case (i.e. there is no force feedback to the structure and the additional control devices are disconnected from the structural system). J_6 measures the maximum forces developed in the control device and is normalized by the peak base shear. J_7 and J_8 are the root mean-square (RMS) values of displacement and base acceleration, respectively. Finally, the energy dissipated by control devices, J_9, is calculated as a percentage of the input excitation energy.

3. SEMIACTIVE CONTROL SYSTEM USING MR DAMPERS

3.1. Control devices and sensors

3.1.1. Nonlinear models for frictional bearings. In this study, two different nonlinear models for the frictional bearings are considered to generate the controller. The originally nonlinear model for the isolated structural system considers the torsional effect so that each bearing force in the same translational direction is different from the others. Based on the original design for frictional bearings, the mathematical form of this type of bearings is formulated by a nonlinear hysteretic model multiplied to the friction force plus a linear re-centering stiffness. In general, a sliding model can be used in this type of frictional bearings and therefore the first estimated model adopts the bilinear model [12] to approach the total bearing forces in either the x- or y-direction. The approximate model translates all bearing forces to the center of mass and neglects the torsional response of all bearings. In other words, all frictional bearings are simplified into two bilinear models in both the x- and y-direction. Moreover, the bilinear model consists of three parameters, pre-yield stiffness, yield displacement and a factor of stiffness reduction for the post-yield stiffness. All parameters are obtained from the uncontrolled response of a single frictional bearing using a nonlinear least-squares method. The model is then fit using the original structural responses without control devices, as shown in Figures 2 and 3. The forces associated with the simplified model of the single frictional bearing are transformed to the center

DOI: 10.1002/stc

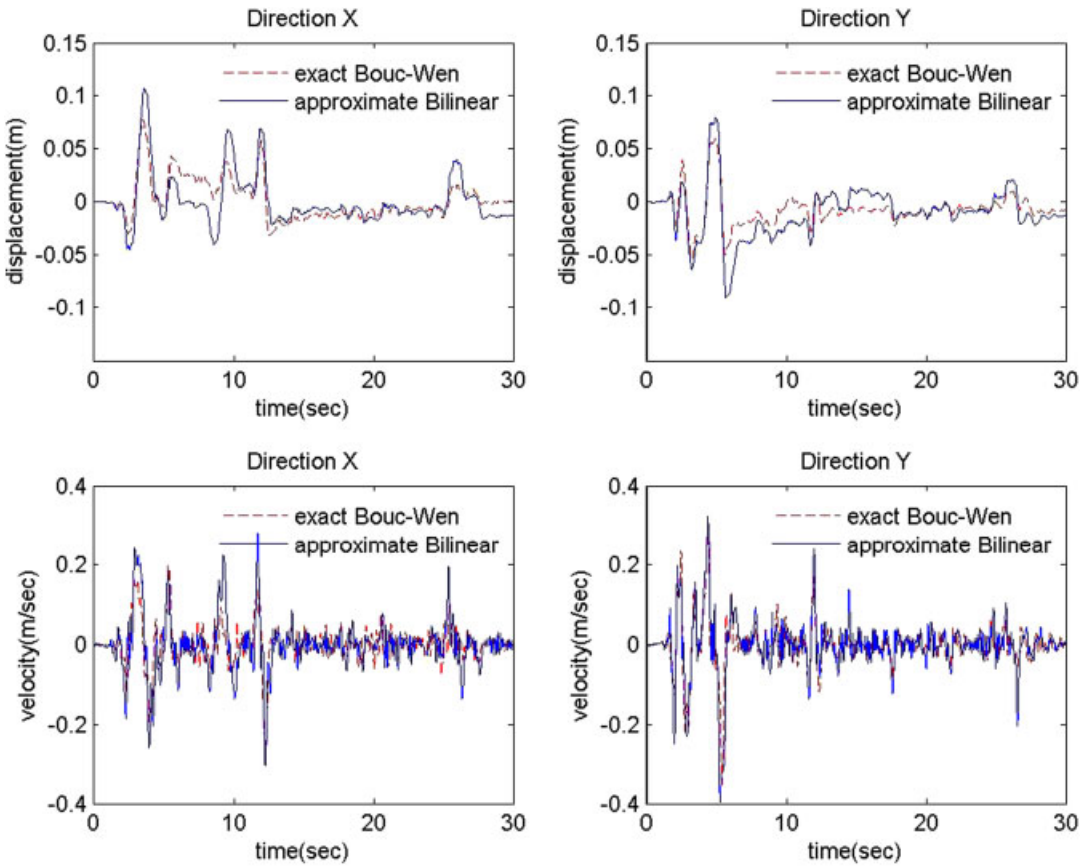

Figure 2. Comparison of the responses of displacement and velocity between the original nonlinear bearings and the approximate bilinear model at the center of mass.

of mass; the resulting fit of the displacement and velocity responses is good, although the hysteretic behavior cannot represent the exact force because of the torsional effect.

The second nonlinear model estimates the nonlinear bearing by utilizing the Bouc–Wen model of the form provided in the benchmark control problem. This model emphasizes a more precise estimate of the bearing forces. Therefore, in the controller design, the nonlinear bearing forces need to be calculated at each time step by using the reduced-order state space system. However, the parameters of the bilinear model and the Bouc–Wen model need to be found in advance. The off-line regression method adopts least-squares optimization using the responses of the displacement and the velocity as the input data and the responses of the force as the output data from the uncontrolled case. After regression, the approximate model using the Bouc–Wen hysteretic model is shown in Figures 4 and 5, which are compared with the original structural responses. By comparing the two nonlinear models, the Bouc–Wen hysteretic model is shown to describe the frictional bearing behavior better than the bilinear model, but requires significant

DOI: 10.1002/stc

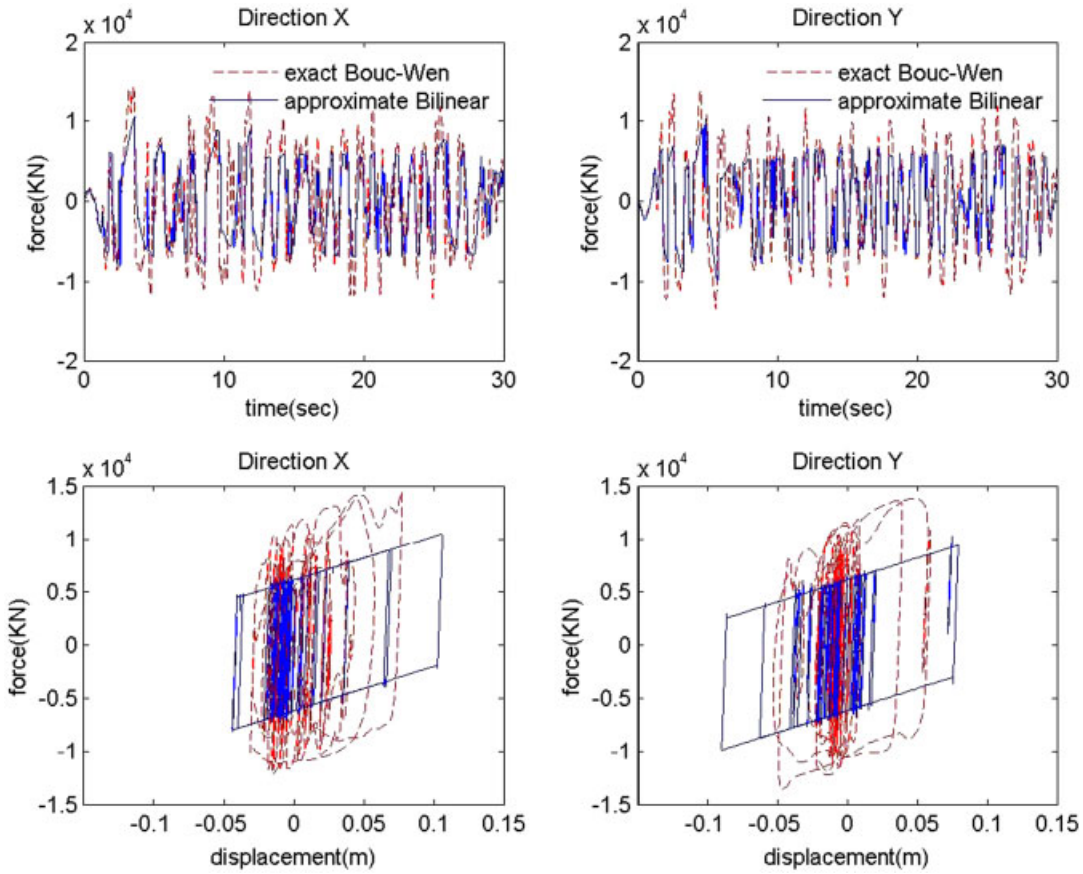

Figure 3. Comparison of the responses of force and hysteretic behavior between the original nonlinear bearings and the approximate bilinear model at the center of mass.

computational resources. Once the nonlinear model for the frictional bearings is determined, model-based control strategies can be designed.

3.1.2. Dynamic and inverse dynamic models for MR damper. An appropriate numerical model that can describe the dynamic behavior of the MR damper is required for the controller design employed. This study herein adopts the Bouc–Wen model [14] for the MR dampers as indicated in the mechanical model shown in Figure 6.

The MR damper model [15] combines the mass and the damping with the Bouc–Wen hysteretic loop inside without considering the spring stiffness. The complete mathematical form is detailed as follows:

$$f_{\text{dev}} = \alpha z_{\text{dev}} + c_{\text{dev}}(\dot{x}_b)\dot{x}_b + m_{\text{dev}}\ddot{x}_b + f_{\text{dev},0} \tag{1}$$

$$c_{\text{dev}}(\dot{x}_b) = a_3\dot{x}_b^3 + a_2\dot{x}_b^2 + a_1\dot{x}_b + a_0 \tag{2}$$

$$\dot{z}_{\text{dev}} = -\gamma_{\text{dev}}|\dot{x}_b||z_{\text{dev}}|z_{\text{dev}}|^{n-1} - \beta_{\text{dev}}\dot{x}_b|z_{\text{dev}}|^n + A_{\text{dev}}\dot{x}_b \tag{3}$$

DOI: 10.1002/stc

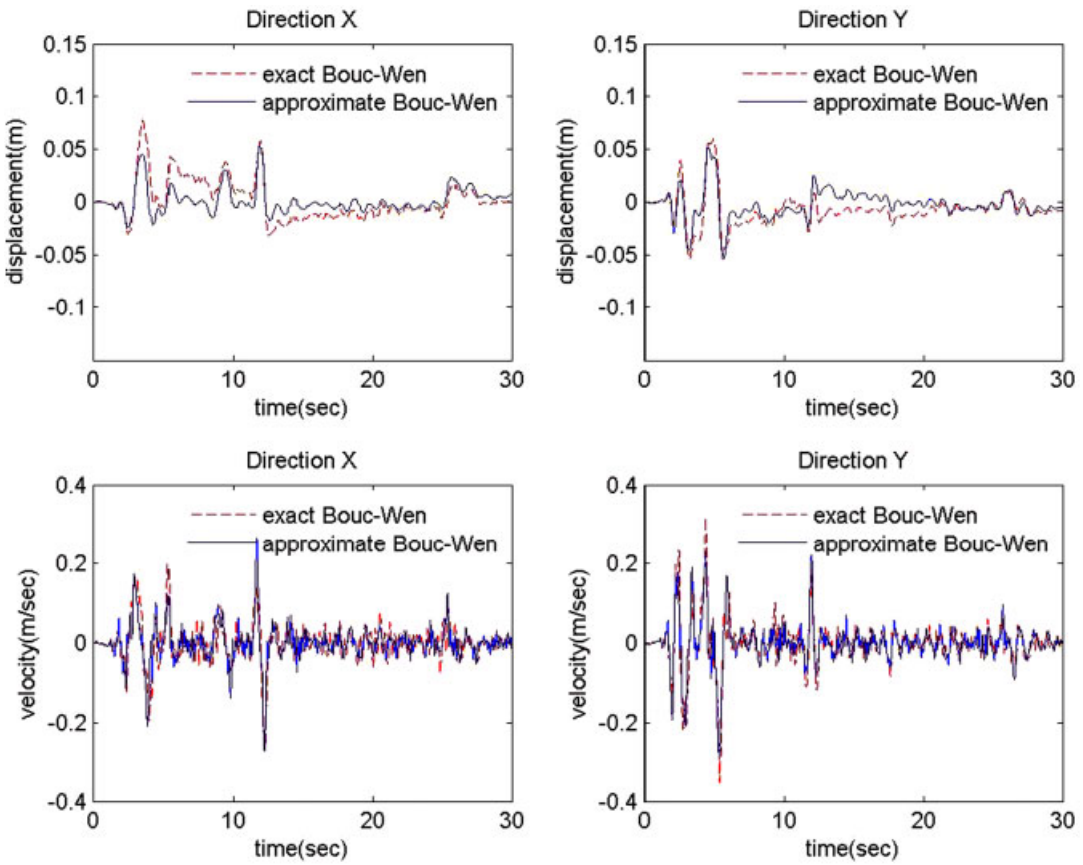

Figure 4. Comparison of the responses of displacement and velocity between the original nonlinear bearings and the approximate Bouc–Wen model at the center of mass.

Here, z_{dev} is the evolutionary variable for the historical dependence of the response from the Bouc–Wen hysteretic model. In general, some researchers suggest that a first-order filter should be added to accommodate the time required to reach the rheological equilibrium and in driving the electromagnet for modeling the MR dampers. Nevertheless, this MR damper model that is used in this study neglects the effect on the saturation of the MR fluid. A least-squares regression method of the MR damper performance tests is used to obtain all coefficients of the MR damper model.

All coefficients of this model depend upon the voltage level, and the driving voltage in this experiment ranges from 0 to 1.2 V. A polynomial function is formed in order to observe the trend of all coefficients related to voltage levels. After using the nonlinear least-squares method to fit all the coefficients as a function of voltage, the proposed modified model was validated using the experimental data of the MR dampers tested in the National Center for Research on Earthquake Engineering (NCREE). The MR dampers used in this test have a force capacity of

DOI: 10.1002/stc

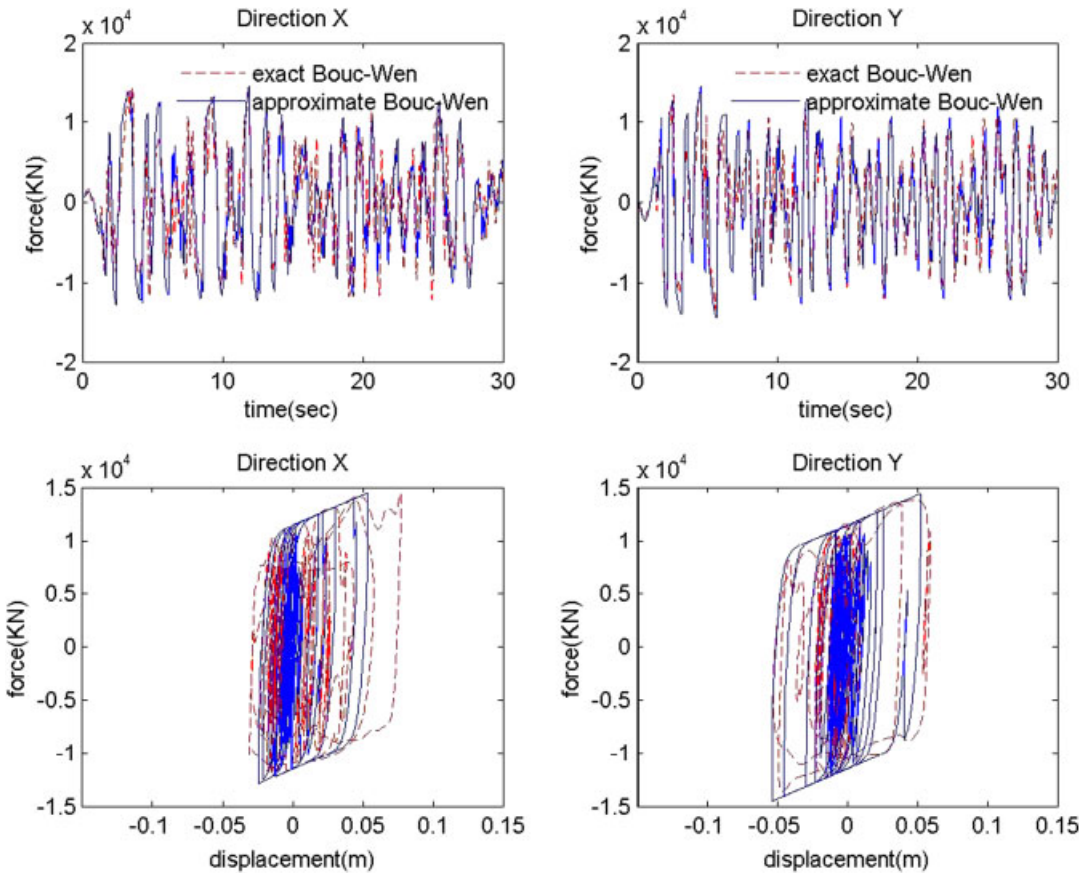

Figure 5. Comparison of the responses of force and hysteretic behavior between the original nonlinear bearings and the approximate Bouc–Wen model at the center of mass.

20 kN with a maximum stroke and a relative velocity of approximately 4 cm and 45 cm/s, respectively [16]. The comparison between experiment and simulation is shown in Figure 7. The test of the MR damper performance is done employing a random stroke and a random voltage with inputs and responses measured.

The coefficients of the MR damper model are adjusted so that it is adequate for the benchmark structure. The output force is amplified 50 times the original control force, and the capacity of the MR damper on the relative responses of velocity and acceleration is appropriately adjusted, where both of them are divided by 3.5. The adjustment implies that the respective capacity has been 3.5 times of original values.

The MR dampers are driven by electrical power that results in a damping force. Owing to the complexity of the MR damper, it is too difficult to estimate an input voltage to the MR damper given a required force. A better way to approach the suitable voltage command with respect to the required force is to use a simplified forward model and to clip the voltage range into

DOI: 10.1002/stc

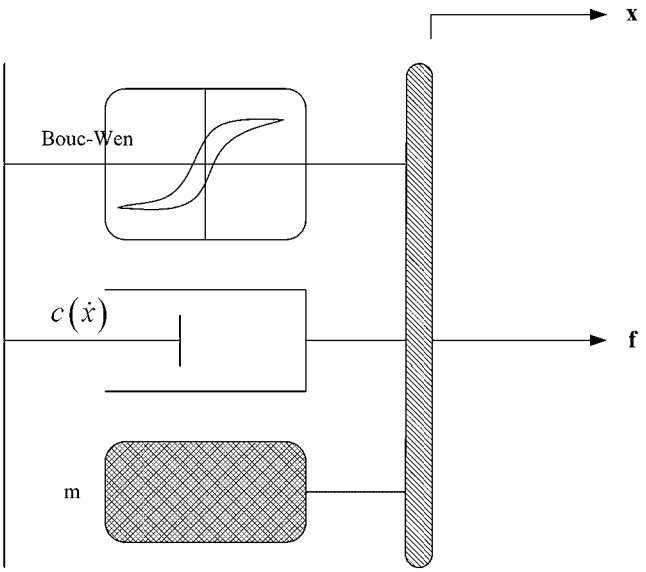

Figure 6. Schematic illustration of the MR damper model.

different levels [17], as shown in Figure 8. Here, the voltage command ranges from 0 to 1.2 V and is divided into 121 levels of equal 0.01 V intervals. Finally, the required voltage with respect to the required force can be generated through the error minimization of the required force and the estimated force from the simplified model. If the method also adopts the Bouc–Wen model as the forward model, computing the required voltage command would be computationally inefficient. Therefore, a simplified model is proposed to efficiently compute the voltage command and is given as

$$f(\dot{x}_b) = \dot{x}_b b_1 \mathrm{e}^{-(b_2|\dot{x}_b|)} \tag{4}$$

in which the two coefficients, b_1 and b_2, are polynomial functions that depend on voltage. Figure 9 represents the illustration of the simplified model that compares with the experimental data. Although this method is not very precise near the origin of the force–velocity plot, it is sufficient in achieving adequate semiactive control effectiveness.

3.1.3. Location of sensors. The control strategy in this case measures the responses of each nonlinear bearing and then generates a feedback control gain with respect to the measurement. The sensors that are selected in the controller design measure the displacement and the velocity of the three DOFs at the center of mass of the base. Practically, it is difficult to measure the responses at the center of mass but these responses can be estimated if there are a few translational sensors placed at locations away from the center of mass (i.e. at the corners or bearings of the structure). Owing to the rigid plate assumption of the floors and the base, the torsional response can be estimated by computing the relationship of the translation and torsional responses. In addition to the measurements at the center of mass of the base, measurements are taken of the relative displacement and velocity at the frictional bearings. In

DOI: 10.1002/stc

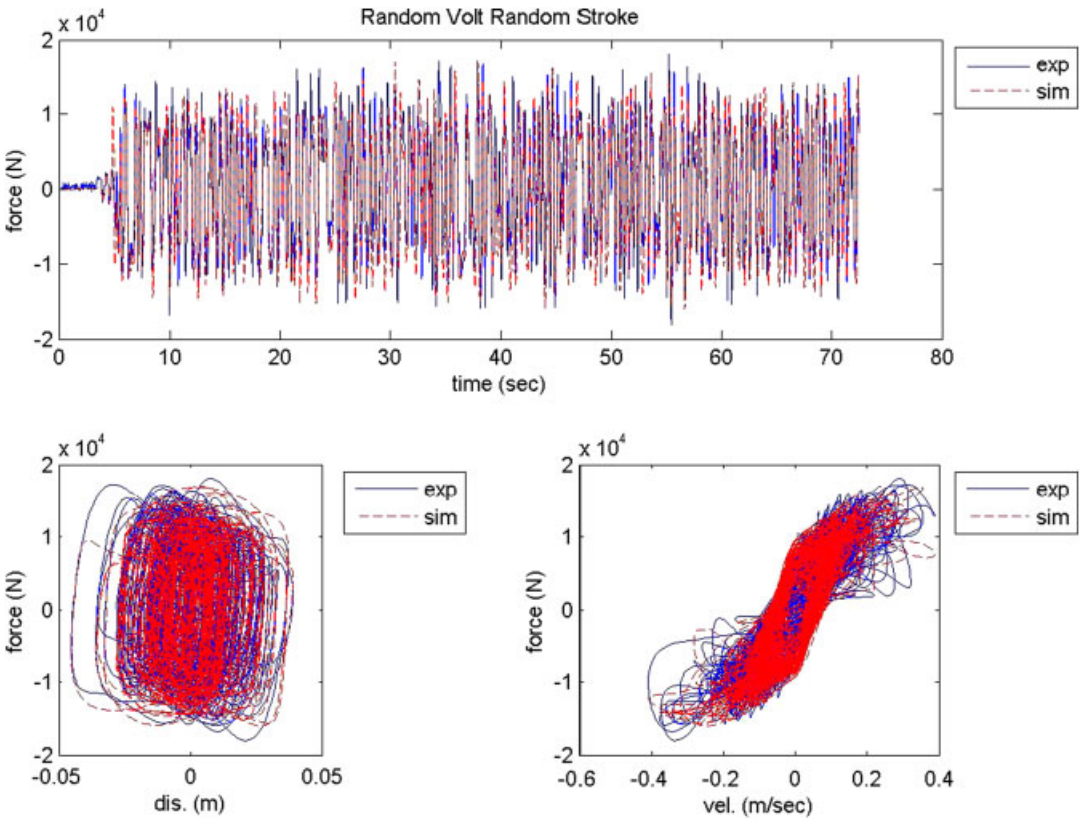

Figure 7. Validation of the model for the MR dampers using the experimentally random voltage and random stroke test.

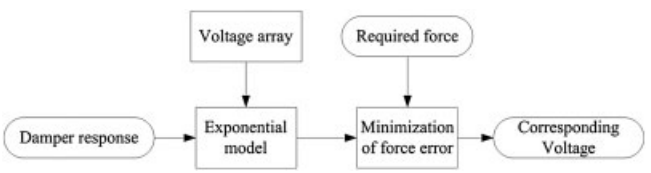

Figure 8. A flowchart of voltage generation for the MR dampers.

total, there are three displacement sensors at the center of mass of the base, three velocity sensors at the same location and 16 sets of relative displacement and velocity sensors at the 8 control device locations if the controller uses the Bouc–Wen model for the reduced-order control system. Each set of sensors for the control devices measures the response in the two principally translational directions. Although the controller combined with the Bouc–Wen

DOI: 10.1002/stc

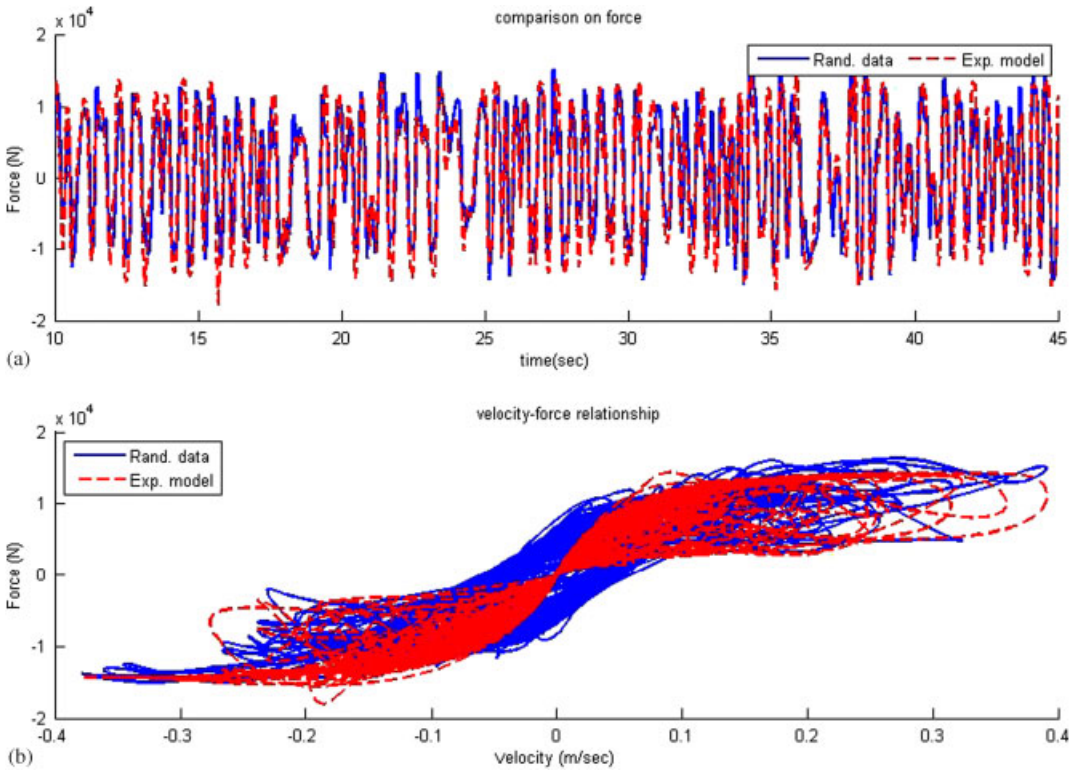

Figure 9. Illustration of the simplified model for the MR dampers to generate the voltage command.

model for the frictional bearings needs the information from each bearing, those responses can be obtained using a transformation matrix based on the rigid plate assumption.

3.2. Control algorithm

3.2.1. Reduced-order model. Using a full model to derive the control force can sufficiently express the structural behavior. However, for nonlinear models, the full-order control algorithm would increase the computational resource. Therefore, a reduced-order model is adopted to determine an appropriate control strategy. The most common method to reduce the order of the system matrices for a linear structure is to adopt the modal approach using the major modes of the linear structure to estimate the structural responses. The reduced-order equation of motion can be expressed as

$$\widehat{\mathbf{M}}\ddot{\mathbf{Z}} + \widehat{\mathbf{C}}\dot{\mathbf{Z}} + \widehat{\mathbf{K}}\mathbf{Z} = -\mathbf{\Phi}^{\mathrm{T}}\mathbf{M}\mathbf{R}(\ddot{\mathbf{U}}_g + \ddot{\mathbf{U}}_b) \tag{5}$$

$$\mathbf{U} = \mathbf{\Phi}\mathbf{Z}, \quad \widehat{\mathbf{M}} = \mathbf{\Phi}^{\mathrm{T}}\mathbf{M}\mathbf{\Phi}, \quad \widehat{\mathbf{C}} = \mathbf{\Phi}^{\mathrm{T}}\mathbf{C}\mathbf{\Phi}, \quad \widehat{\mathbf{K}} = \mathbf{\Phi}^{\mathrm{T}}\mathbf{K}\mathbf{\Phi} \tag{6}$$

DOI: 10.1002/stc

where Φ is the modal matrix related to the selected mode shapes of the superstructure. In this case, only the first three modes are selected, which allows inclusion of modes with natural periods that are larger than 0.5 s. The first three modes correspond to the first x-translational, first y-translational and first z-rotational modes. To avoid a singular matrix occurring in the computation of the structural responses, the reduced-order mass matrix is multiplied by the original total lumped mass from the eighth story to the first story in each diagonal term. Similarly, the damping matrix, the stiffness matrix and the load influence matrix are also needed to make similar modifications. Finally, the state space equation can be reformulated as

$$\dot{\mathbf{X}}_r(t) = \mathbf{A}_r\mathbf{X}_r(t) + \mathbf{B}_r\mathbf{u}_r(t) + \mathbf{E}\ddot{\mathbf{U}}_g(t) \tag{7}$$

$$\mathbf{A}_r = \begin{bmatrix} \mathbf{0} & \mathbf{I} \\ -\bar{\mathbf{M}}_r^{-1}\bar{\mathbf{K}}_r & -\bar{\mathbf{M}}_r^{-1}\bar{\mathbf{C}}_r \end{bmatrix},\ \mathbf{B}_r = \begin{bmatrix} \mathbf{0} \\ \mathbf{I} \end{bmatrix},\ \mathbf{E}_r = \begin{bmatrix} \mathbf{0} \\ -\begin{Bmatrix} \boldsymbol{\Phi}^{\mathrm{T}}\mathbf{M}\mathbf{R} \\ \mathbf{R}^{\mathrm{T}}\boldsymbol{\Phi}\mathbf{M}\boldsymbol{\Phi}^{\mathrm{T}}\mathbf{R} + \mathbf{M}_b \end{Bmatrix} \end{bmatrix} \tag{8}$$

$$\bar{\mathbf{M}}_r = \begin{bmatrix} \widehat{\mathbf{M}} & \boldsymbol{\Phi}^{\mathrm{T}}\mathbf{M}\mathbf{R} \\ \mathbf{R}^{\mathrm{T}}\mathbf{M}\boldsymbol{\Phi} & \mathbf{R}^{\mathrm{T}}\boldsymbol{\Phi}\mathbf{M}\boldsymbol{\Phi}^{\mathrm{T}}\mathbf{R} + \mathbf{M}_b \end{bmatrix},\ \bar{\mathbf{C}}_r = \begin{bmatrix} \widehat{\mathbf{C}} & \mathbf{0} \\ \mathbf{0} & \mathbf{C}_b \end{bmatrix} \tag{9}$$

$$\bar{\mathbf{K}}_r = \begin{bmatrix} \widehat{\mathbf{K}} & \mathbf{0} \\ \mathbf{0} & \mathbf{K}_b \end{bmatrix},\ \mathbf{u}_r = \mathbf{f}_{\mathrm{est},b} + \mathbf{f}_{\mathrm{device}},\ \mathbf{X}_r = [\mathbf{Z}^{\mathrm{T}}\ \mathbf{X}_b^{\mathrm{T}}\ \dot{\mathbf{Z}}^{\mathrm{T}}\ \dot{\mathbf{X}}_b^{\mathrm{T}}]^{\mathrm{T}} \tag{10}$$

in which $\mathbf{A}_r$, $\mathbf{B}_r$ and $\mathbf{E}_r$ are system matrices with 12 states and $f_{\mathrm{est},b}$ indicates the resulting estimated nonlinear force from the total bearing force in the x- and y-direction. To simplify the control strategy for the nonlinear approach case, two types of nonlinear models have been generated to estimate the bearing force in this study based on the relationship of the force *versus* the relative displacement at the center of mass as explained in Section 3.1.

3.2.2. Control algorithm combined with two nonlinear bearing models. To develop the control strategy for the semiactive control devices, an optimal direct output feedback control algorithm [6–8] is employed. Generally, model-based control algorithms always utilize the full- or reduced-order structural system to obtain a control gain or several control gains related to the real state vector. The full-state direct feedback method cannot be realized in real structures because of the limitation in monitoring all the states of the structure. Therefore, most of model-based control algorithms depend on a reduced-order model to estimate the full-state vector. In this case, instead of estimating the full-state vector, the required control force is calculated using the output measurements directly. First, the reduced-order state space equations are formulated using the previously discussed methods and the measurement output is given as

$$\mathbf{Y}_m(t) = \mathbf{C}_r\mathbf{X}_r(t) \tag{11}$$

DOI: 10.1002/stc

Here, $\mathbf{C}_r$ is the measurement matrix corresponding to the sensor location. In this control case, $\mathbf{Y}_m$ is a six-by-one vector, including three displacement and three velocity responses on the center of mass at the base, respectively.

Since this controller is similar to the classic optimal control algorithm, the objective function can be described as

$$J = \int_0^\infty [\mathbf{X}_r^{\mathrm{T}}(t)\mathbf{Q}_w\mathbf{X}_r(t) + \mathbf{u}_{\mathrm{dev}}^{\mathrm{T}}(t)\mathbf{R}_w\mathbf{u}_{\mathrm{dev}}(t)]\,\mathrm{d}t \tag{12}$$

where the subscript r denotes the vector derived from the reduced-order model, the subscript dev denotes the control force resulting from the control devices and the subscript w denotes the weighting. This objective function is similar to that of the conventional H_2 optimal control algorithm [11]. Since the control gain is related only to the output measurement, the objective function needs to be modified as

$$J = \mathbf{X}_{r,0}^{\mathrm{T}}\left[\int_0^\infty (\mathrm{e}^{(\mathbf{A}_r+\mathbf{B}_r\mathbf{G}\mathbf{C}_r)t})^{\mathrm{T}}(\mathbf{Q}_w + \mathbf{C}_r^{\mathrm{T}}\mathbf{G}^{\mathrm{T}}\mathbf{R}_w\mathbf{G}\mathbf{C}_r)(\mathrm{e}^{(\mathbf{A}_r+\mathbf{B}_r\mathbf{G}\mathbf{C}_r)t})\,\mathrm{d}t\right]\mathbf{X}_{r,0} \tag{13}$$

and the assumed control force as

$$\mathbf{u}_r(t) = \mathbf{G}\mathbf{C}_r\mathbf{X}_r(t) \tag{14}$$

where $\mathbf{X}_{r,0}$ indicates the initial state of the reduced-order model under random initial conditions. To simplify the objective function, the integral term can be transformed into

$$\mathbf{H} = \int_0^\infty (\mathrm{e}^{(\mathbf{A}_r+\mathbf{B}_r\mathbf{G}\mathbf{C}_r)t})^{\mathrm{T}}(\mathbf{Q}_w + \mathbf{C}_r^{\mathrm{T}}\mathbf{G}^{\mathrm{T}}\mathbf{R}_w\mathbf{G}\mathbf{C}_r)(\mathrm{e}^{(\mathbf{A}_r+\mathbf{B}_r\mathbf{G}\mathbf{C}_r)t})\,\mathrm{d}t \tag{15}$$

Since the initial condition of the state vector is random, the objective function can be substituted into an expected form as

$$\widehat{J} = E[J] = E[\mathbf{X}_{r,0}^{\mathrm{T}}\mathbf{H}\mathbf{X}_{r,0}] = \mathrm{tr}(\mathbf{H}\mathbf{X}_{r,0}^{e}) \tag{16}$$

$$\mathbf{X}_{r,0}^{e} = E[\mathbf{X}_{r,0}\mathbf{X}_{r,0}^{\mathrm{T}}] \tag{17}$$

where $E[]$ denotes the expectation and tr() denotes the trace of a matrix. To optimize the control force using the expected objective function, the Lagrangian multipliers need to be used in the expected function of the following form:

$$\widehat{J}_{\mathrm{new}} = \mathrm{tr}(\mathbf{H}\mathbf{X}_{r,0}^{e}) + \mathrm{tr}\{\mathbf{L}[(\mathbf{A}_r + \mathbf{B}_r\mathbf{G}\mathbf{C}_r)^{\mathrm{T}}\mathbf{H} + \mathbf{H}(\mathbf{A}_r + \mathbf{B}_r\mathbf{G}\mathbf{C}_r) + (\mathbf{Q}_w + \mathbf{C}_r^{\mathrm{T}}\mathbf{G}^{\mathrm{T}}\mathbf{R}_w\mathbf{G}\mathbf{C}_r)]\} \tag{18}$$

where $\mathbf{L}$ is equal to the Lagrangian multiplier matrix. Since the objective function is in quadratic form, the minimum value of this function definitely exists as long as the weighting matrices $\mathbf{Q}_w$ and $\mathbf{R}_w$ are positive semi-definite and positive definite, respectively. To find the minimum of the objective function, the derivative of the function with respect to the Lagrangian multipliers, the matrix $\mathbf{H}$ and the control gain can be expressed as follows:

$$\frac{\partial\widehat{J}_{\mathrm{new}}}{\partial\mathbf{L}} = (\mathbf{A}_r + \mathbf{B}_r\mathbf{G}\mathbf{C}_r)^{\mathrm{T}}\mathbf{H} + \mathbf{H}(\mathbf{A}_r + \mathbf{B}_r\mathbf{G}\mathbf{C}_r) + (\mathbf{Q}_w + \mathbf{C}_r^{\mathrm{T}}\mathbf{G}^{\mathrm{T}}\mathbf{R}_w\mathbf{G}\mathbf{C}_r) = 0 \tag{19}$$

$$\frac{\partial\widehat{J}_{\mathrm{new}}}{\partial\mathbf{H}} = \mathbf{X}_{r,0}^{e} + \mathbf{L}(\mathbf{A}_r + \mathbf{B}_r\mathbf{G}\mathbf{C}_r)^{\mathrm{T}} + (\mathbf{A}_r + \mathbf{B}_r\mathbf{G}\mathbf{C}_r)\mathbf{L} = 0 \tag{20}$$

DOI: 10.1002/stc

$$\frac{\partial \widehat{J}_{\text{new}}}{\partial \mathbf{G}} = 2\mathbf{B}_r^{\mathrm{T}}\mathbf{H}\mathbf{L}\mathbf{C}_r^{\mathrm{T}} + 2\mathbf{R}_w\mathbf{G}\mathbf{C}_r\mathbf{L}\mathbf{C}_r^{\mathrm{T}} = 0 \tag{21}$$

Here, the first two equations are in the form of the Lyapunov function and the last equation is directly related to the control gain. To solve these equations, the first step is to determine the initial control gain at a time close to infinity, and then the second step is to iteratively solve the two Lyapunov functions until the control gain of matrix **G** converges. Finally, the time-invariant control gain can be determined but the control algorithm does not consider the nonlinear effect from the frictional bearings. Therefore, the control algorithm must be partially modified to consider the combination of the nonlinear bearing model.

To consider the bilinear model as the nonlinear frictional bearings, two stiffness slopes, pre-yield stiffness and post-yield stiffness need to be introduced into the system matrix $\mathbf{A}_r$, which can be described as

$$\mathbf{A}_r(t) = \begin{bmatrix} \mathbf{0} & \mathbf{I} \\ -\bar{\mathbf{M}}_r^{-1}\bar{\mathbf{K}}_r(t) & -\bar{\mathbf{M}}_r^{-1}\bar{\mathbf{C}}_r \end{bmatrix}, \quad \bar{\mathbf{K}}_r(t) = \begin{bmatrix} \widehat{\mathbf{K}} & \mathbf{0} \\ \mathbf{0} & \mathbf{K}_{b,\text{linear}} + \mathbf{K}_{b,\text{nonlinear}}(t) \end{bmatrix} \tag{22}$$

where $\mathbf{K}_{b,\text{nonlinear}}$ is a nonlinear term with respect to the bilinear model. Because the approximate nonlinear model depends on the responses of the center of mass at the base and focuses on the translational responses in the x- and y-direction, there are only four combinations for the time-variant matrix $\mathbf{A}_r(t)$ (two slopes for the x-direction and two slopes for the y-direction). Although this control algorithm is derived from the linear definition, the control gain at each time step based on this assumption is initially linear at the beginning time point of the time interval. This methodology is referred to as the linear approach for nonlinear control problems [18]. Therefore, the four control gains can be generated in advance as long as the pre-yield stiffness and post-yield stiffness are known. However, the displacement and velocity responses determine the slope in the current position of the segments in this bilinear model. One of the four control gains will be selected during the simulation based on the current status of the friction bearing. Using switching gains may induce sudden impulsive forces in the active control devices, but the semiactive control devices cannot input energy to structures; therefore, the phenomenon will not happen in this control strategy.

It is computationally inefficient to calculate the control gain based on the highly nonlinear hysteretic model if it is embedded in the $\mathbf{A}_r$ matrix. Hence, the second way to approach the computation of the nonlinear control force focuses on the time-invariant system matrix $\mathbf{A}_r$ to generate the control gain. The compensated force coming from the nonlinear terms of the frictional bearings is added to the optimal control force from the control gain as well as

$$\mathbf{u}_r(t) = \mathbf{G}\mathbf{Y}_m(t) - \mu N\mathbf{z}_b \tag{23}$$

$$\dot{z}_{b,j} = \frac{1}{u^y}[\alpha\dot{x}_{b,j} - (\gamma|\dot{x}_{b,j}||z_{b,j}|z_{b,j} + \beta\dot{u}z_{b,j}^2)] \tag{24}$$

in which j denotes the j-th component with respect to the control devices, μ is the coefficient of friction, N is the normal force of each bearing, $\mathbf{z}_b$ is the hysteretic variable, u^y is the yield displacement, $\mathbf{x}_b$ is the relative displacement of each bearing and α, β and γ are the parameters of the Bouc–Wen model [14]. All parameters are found off-line using the data from the uncontrolled simulation. The nonlinear control force also contains a directional effect and needs to be calculated at each time point.

DOI: 10.1002/stc

4. NUMERICAL SIMULATION RESULTS

4.1. Modified evaluation criteria

The performance indices, i.e. J_1–J_9, are provided in the benchmark description [9] and used to compare the control strategies with each other if the placement of the measurement and control devices are set as the same. However, the control performance is not easily compared by these indices if the control strategies used different control algorithms combined with different measurements and different types of control devices. Here, a clear and easy-to-read method

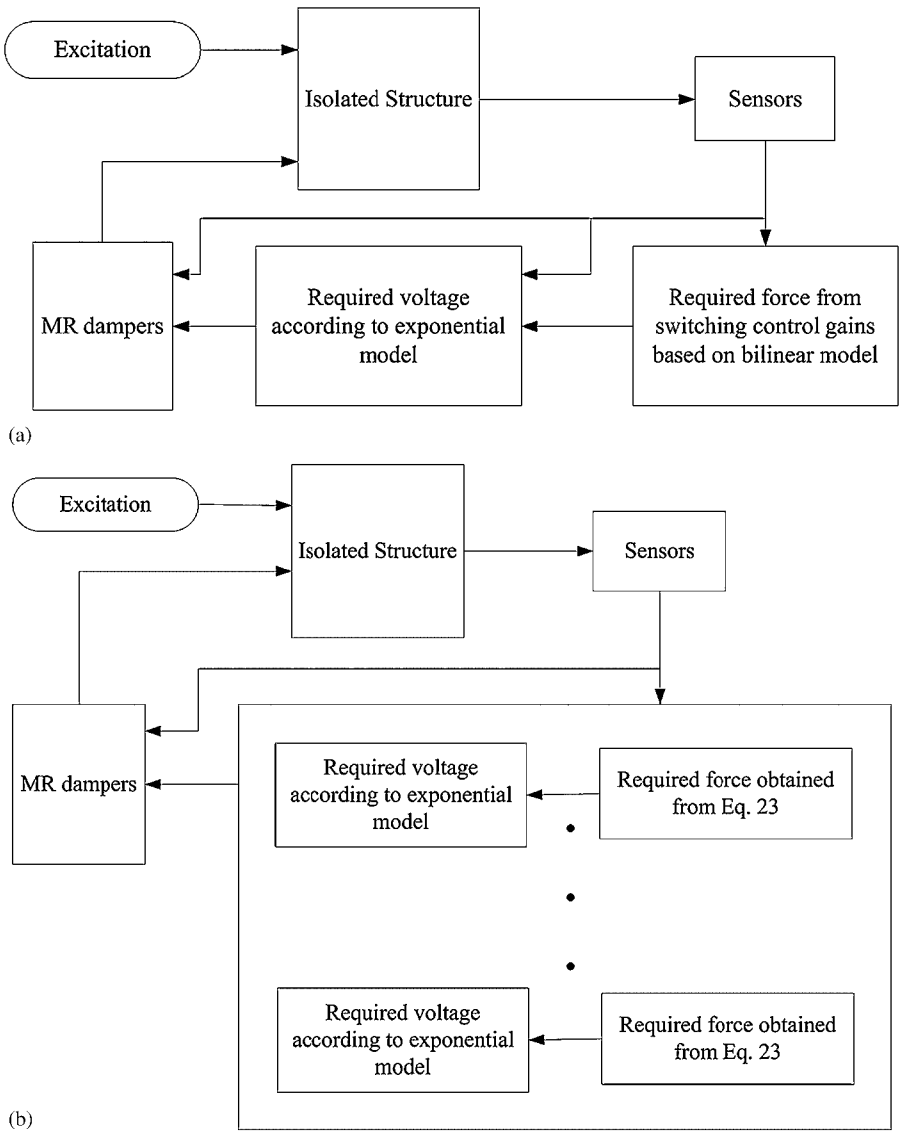

Figure 10. (a) Control strategy—using bilinear model and (b) control strategy—using Bouc–Wen model.

DOI: 10.1002/stc

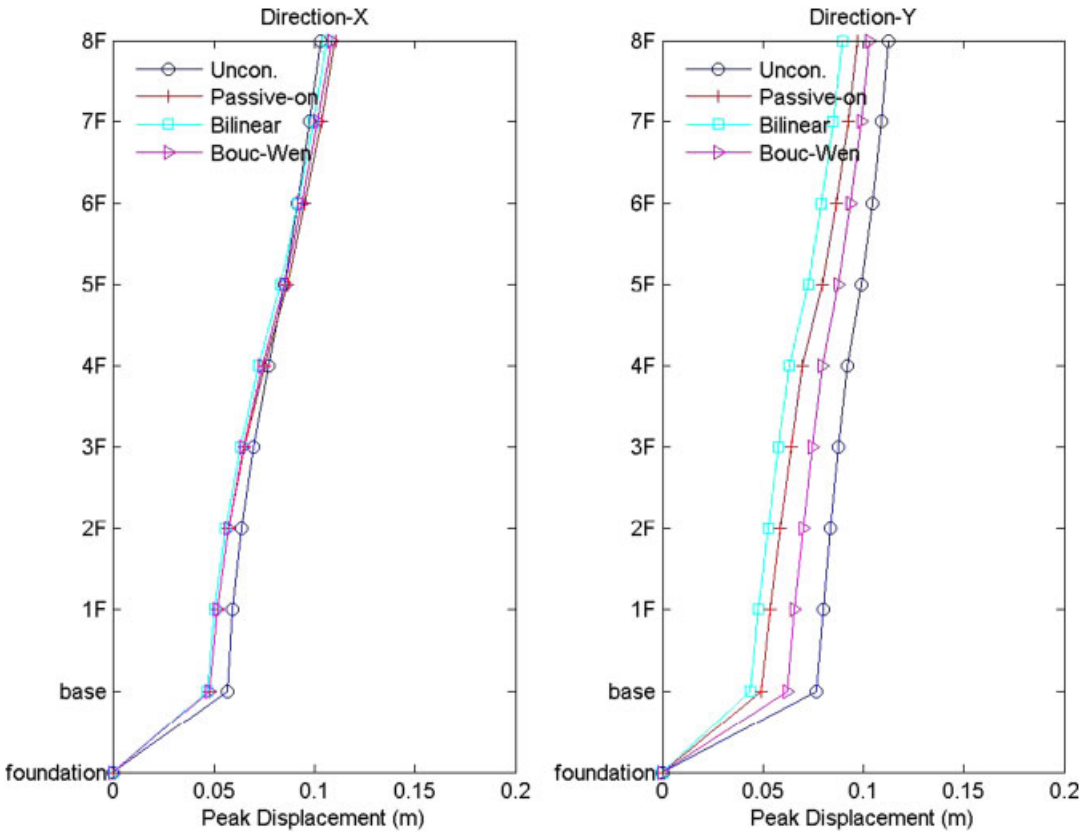

Figure 11. Responses of peak displacement in the x- and y-direction using the proposed MR damper under the excitation of the El Centro earthquake record (FP-y and FN-x).

using these indices is proposed to distinguish one control strategy from the others. First, the modified index J_{1m} is used to consider the relation of the peak base and drift displacements to the peak control force. The second modified index J_{2m} is used to demonstrate the relation of the peak base shear, the peak floor acceleration and the RMS floor acceleration to the energy dissipation. These two modified indices are demonstrated as follows:

$$J_{1m} = \frac{(1 - J_3) + (1 - J_4)}{J_6} \tag{25}$$

$$J_{2m} = \frac{(1 - J_1) + (1 - J_5) + (1 - J_8)}{J_9} \tag{26}$$

These performance indices consider the control performance with respect to the reduction of the structural responses. A reasonable and effective control strategy is to be able to reduce the displacements while increasing the accelerations only slightly. Furthermore, large values, instead of smaller values, of these two indices show better performance.

DOI: 10.1002/stc

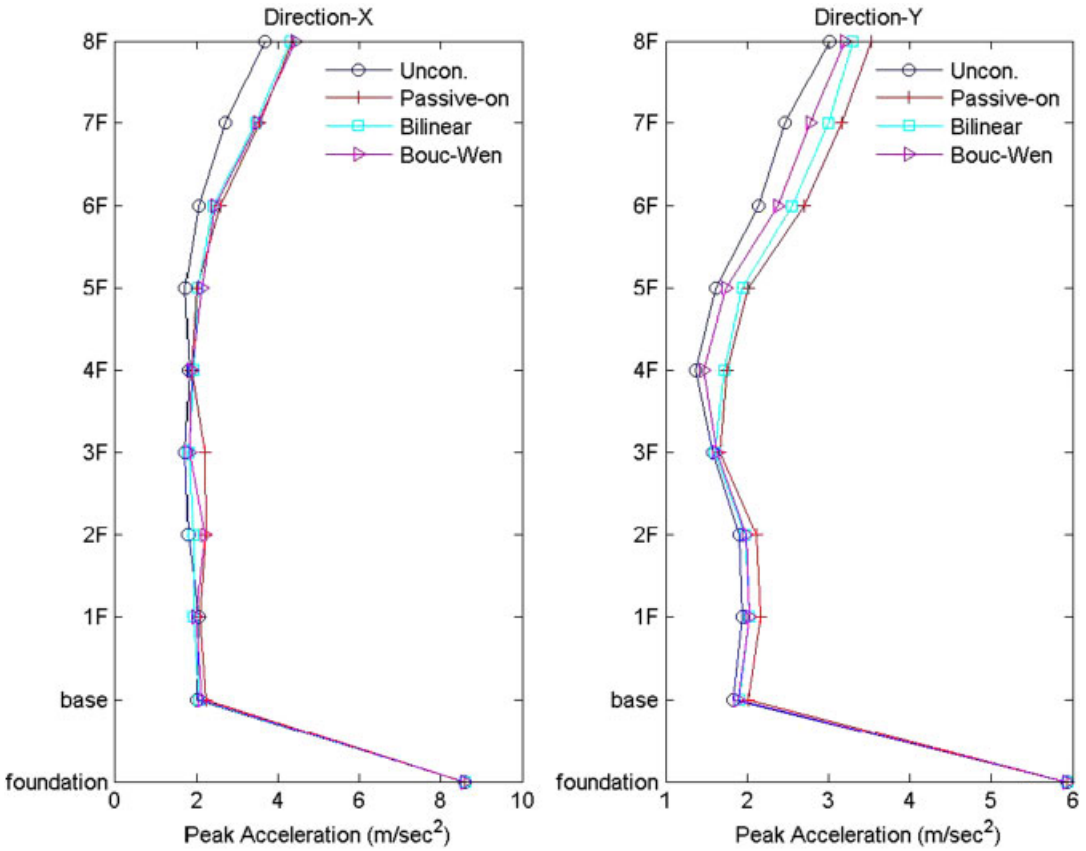

Figure 12. Responses of peak acceleration in the x- and y-direction using the proposed MR damper under the excitation of the El Centro earthquake record (FP-y and FN-x).

4.2. Simulation results

4.2.1. Control strategies. In this study, two control strategies are examined in this control benchmark problem. The first one (see Figure 10(a)) switches four control gains based on the bilinear model at the center of mass to generate the required force, and then the required voltage for the MR dampers is calculated through the flowchart shown in Figure 8. The damper force can be obtained either from the proposed MR damper model or from the benchmark MR damper model. The second one calculates the required control force using Equation (23) and then generates the required voltage by the same way. Similarly, two MR damper models are also evaluated in this control strategy. The largest difference between the two control strategies is the force generation. The first one is to sense the structural response at the center of mass and distribute the force to each damper location. The second one is to calculate the required control force individually with respect to the dampers.

4.2.2. Control case using proposed MR damper model. The nonlinear control algorithm using the proposed model for MR dampers includes two methods: one uses the bilinear model to estimate

DOI: 10.1002/stc

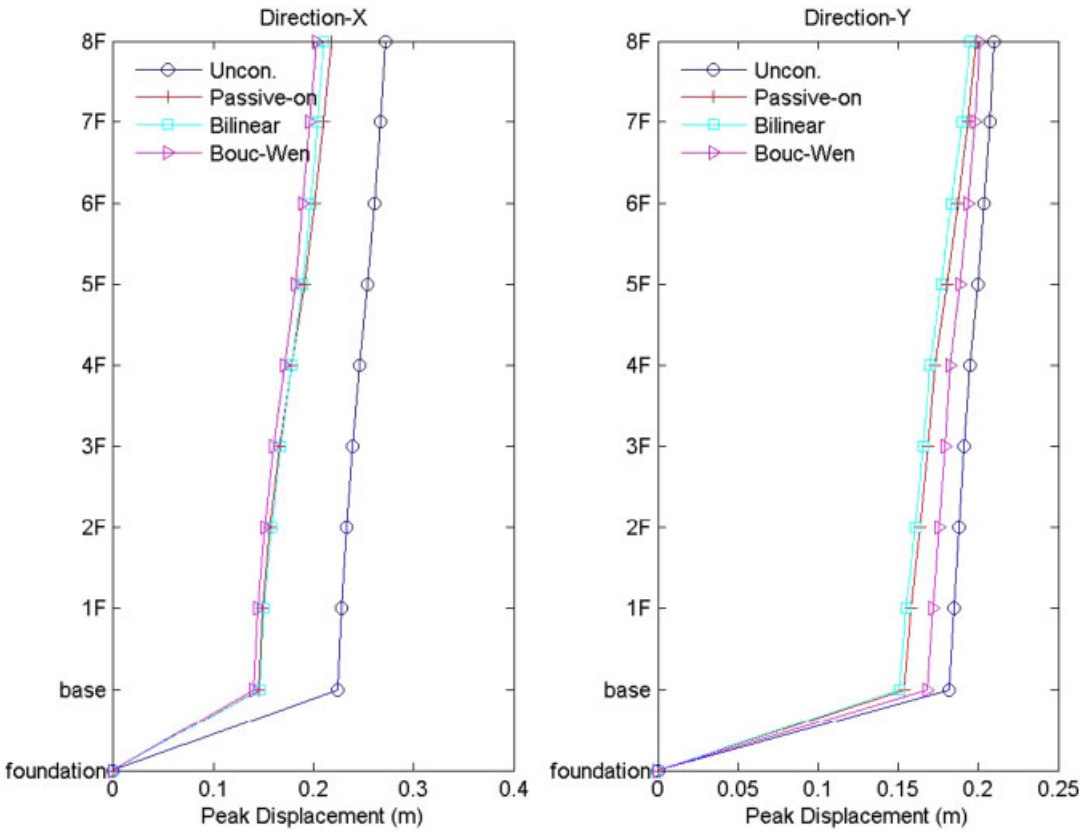

Figure 13. Responses of peak displacement in the *x*- and *y*-direction using the proposed MR damper under the excitation of the Kobe earthquake record (FP-*y* and FN-*x*).

the nonlinear response of the frictional bearings, while the other uses the Bouc–Wen model to approximate the nonlinear forces of the frictional bearings. An effective controller will have large reductions in the base displacement without significantly increasing the floor accelerations. The two semiactive control algorithms are also compared with the passive-on case in which the MR dampers act as passive devices with the maximum voltage command. Figure 11 shows the comparison of the peak displacement responses at each floor and the base in the case of the El Centro earthquake record.

The results show that either the passive-on control strategy or two semiactive control strategies produce similar responses to the uncontrolled case in the *x*-direction. However, in the *y*-direction, the semiactive control strategy using the bilinear model to approach the nonlinear bearing force produces better results than the other control strategies. The reason for this phenomenon is that the goal of this control strategy is to reduce only the base displacement. Although the control strategy using the bilinear model for nonlinear bearings effectively reduces the base displacement, the base acceleration is slightly increased compared with the uncontrolled case, as shown in Figure 12.

DOI: 10.1002/stc

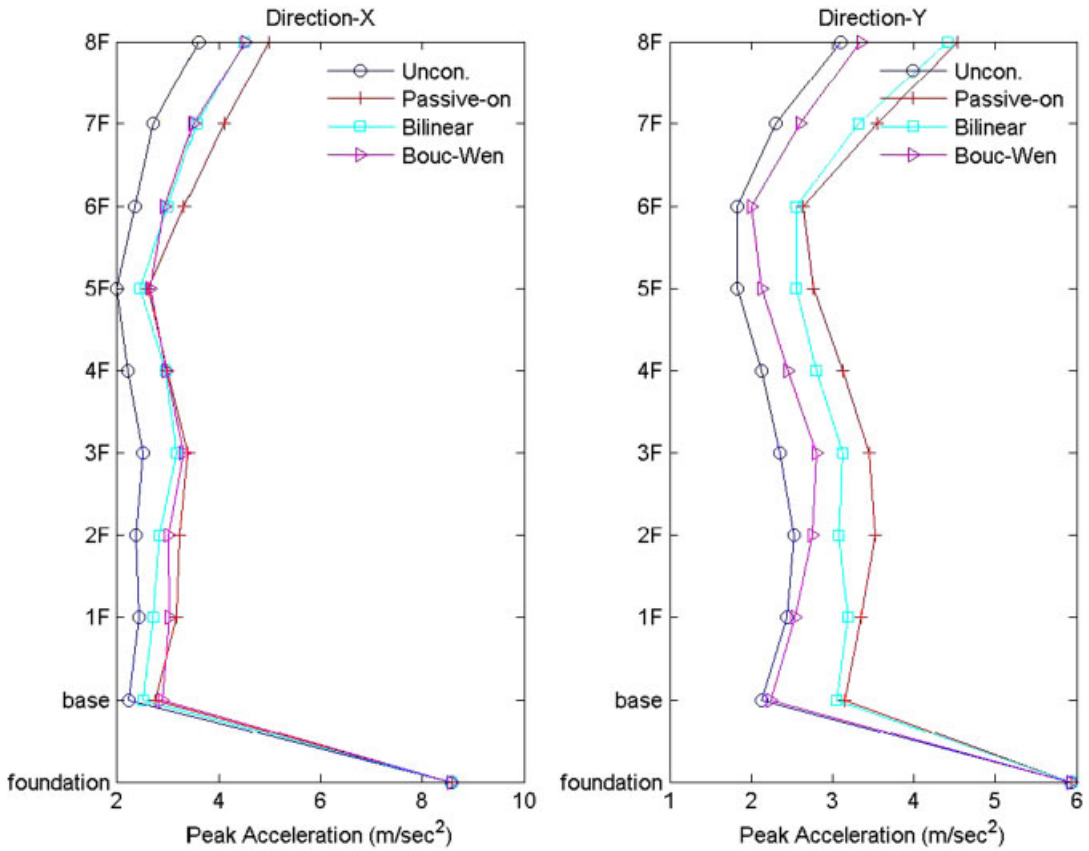

Figure 14. Responses of peak acceleration in the x- and y-direction using the proposed MR damper under the excitation of the Kobe earthquake record (FP-y and FN-x).

Table I. Results of control strategies using the proposed MR dampers (FP-x and FN-y).

J_{1m}		Newhall	Sylmar	El Centro	Rinaldi	Kobe	Jiji	Erzinkan
Semiactive	Passive-on	−0.14	0.66	0.13	0.49	−0.65	2.22	0.73
	Bilinear	0.06	1.30	0.01	0.45	−0.57	2.33	−0.07
	Bouc–Wen	0.01	0.47	0.36	0.17	−1.19	1.90	−0.12
J_{2m}		Newhall	Sylmar	El Centro	Rinaldi	Kobe	Jiji	Erzinkan
Semiactive	Passive-on	−1.08	−1.08	−3.27	−2.94	−2.38	0.37	−1.09
	Bilinear	−1.14	−0.85	−2.78	−2.34	−2.05	0.64	−1.17
	Bouc–Wen	−0.94	−0.51	−2.21	−1.54	−2.12	0.73	−0.08

To compare the influence of the major near-fault excitation with the control strategies, the control case under the excitation of the Kobe earthquake is used and is shown in Figures 13 and 14.

DOI: 10.1002/stc

Table II. Results of control strategies using the proposed MR dampers (FP-y and FN-x).

J_{1m}		Newhall	Sylmar	El Centro	Rinaldi	Kobe	Jiji	Erzinkan
Semiactive	Passive-on	−0.14	0.66	0.13	0.49	−0.65	2.22	0.73
	Bilinear	0.06	1.30	0.01	0.45	−0.57	2.33	−0.07
	Bouc–Wen	0.01	0.47	0.36	0.17	−1.19	1.90	−0.12
J_{2m}		Newhall	Sylmar	El Centro	Rinaldi	Kobe	Jiji	Erzinkan
Semiactive	Passive-on	−1.08	−1.08	−3.27	−2.94	−2.38	0.37	−1.09
	Bilinear	−1.14	−0.85	−2.78	−2.34	−2.05	0.64	−1.17
	Bouc–Wen	−0.94	−0.51	−2.21	−1.54	−2.12	0.73	−0.08

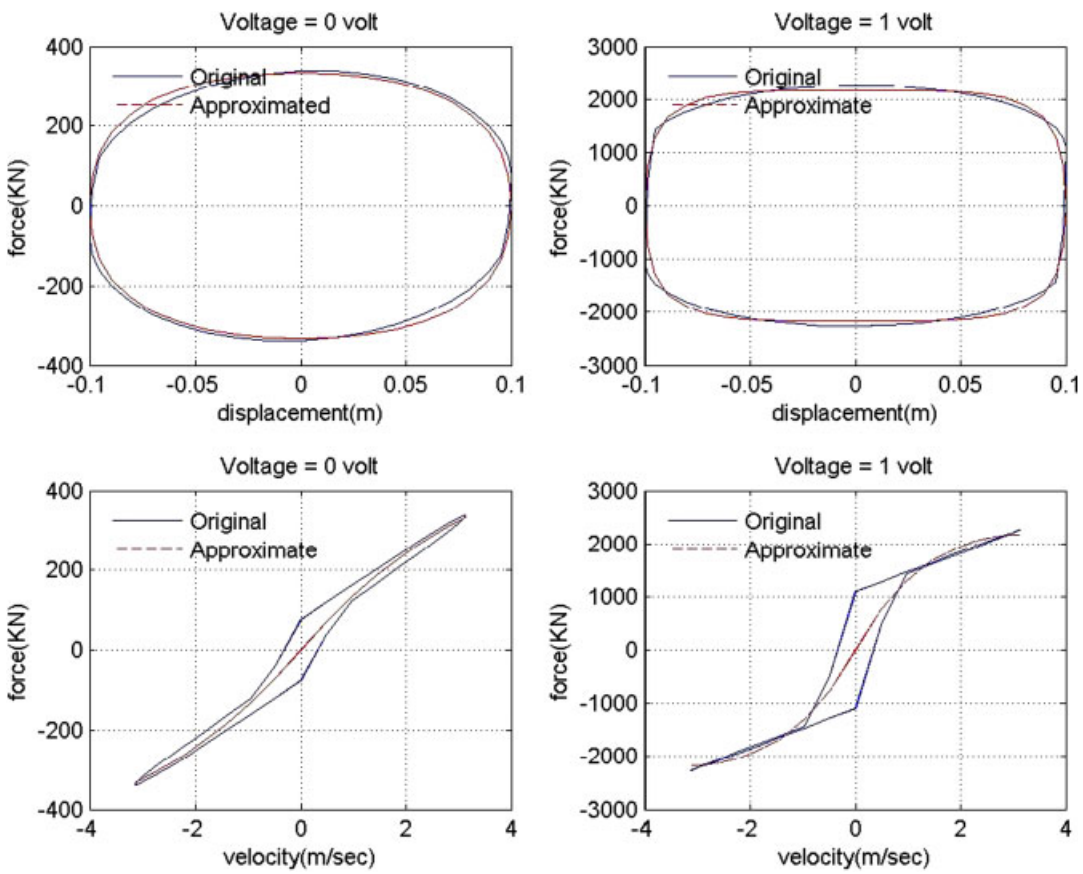

Figure 15. Simplified model for the MR dampers of the benchmark control problem.

In this case, both of the semiactive control strategies mitigate the displacement responses with a slight increase in the acceleration response for the Kobe earthquake record. However, the increase is still in the acceptable range. The overall comparison of the control performance using the modified indices is reported in Tables I and II.

DOI: 10.1002/stc

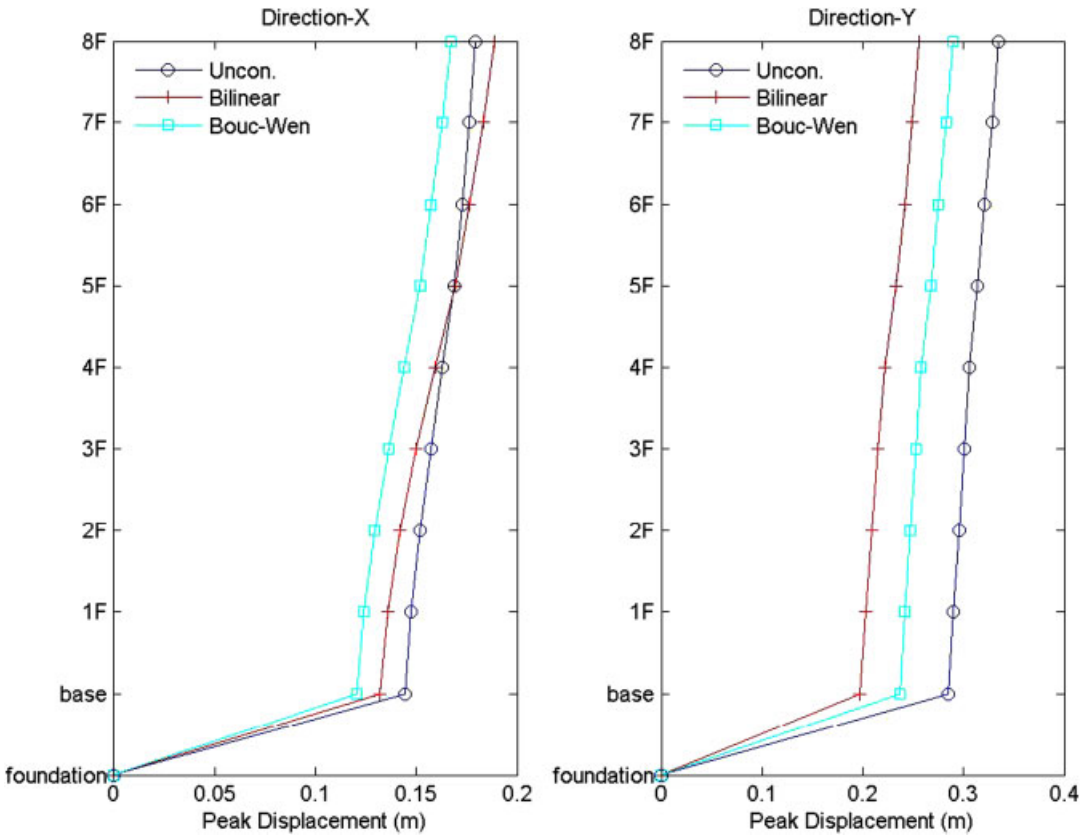

Figure 16. Responses of peak displacement in the x- and y-direction using the MR dampers of the benchmark control problem under the excitation of the Newhall earthquake record (FP-x and FN-y).

4.2.3. Control case using the benchmark MR damper model. The second part of the nonlinear control algorithm is to use the MR dampers that are provided by the benchmark control problem and to combine with the aforementioned control algorithm. In this control case, the voltage generator used to drive the MR dampers adopts the same method used for the proposed MR dampers. Here, only two levels of voltage commands are considered: the maximum voltage (1.0 V) and the minimum voltage (0 V).

The simplified model (see Figure 15) is found from the forward model provided by the benchmark control problem. After controlling the isolated building using the control algorithm combined with the bilinear model or the Bouc–Wen model for nonlinearly frictional bearings, the results show that the control algorithm combined with the Bouc–Wen model is more suitable for this type of MR damper. The reason is that the control performance demonstrates a higher reduction in peak base displacement without inducing much acceleration response as compared with the other control strategy in Figures 16 and 17. Similarly, Tables III and IV represent the modified performance indices to evaluate these two control strategies.

In summary, the results of the two semiactive control strategies reveal that the control effectiveness is very close to the sample control strategy in the original benchmark control

DOI: 10.1002/stc

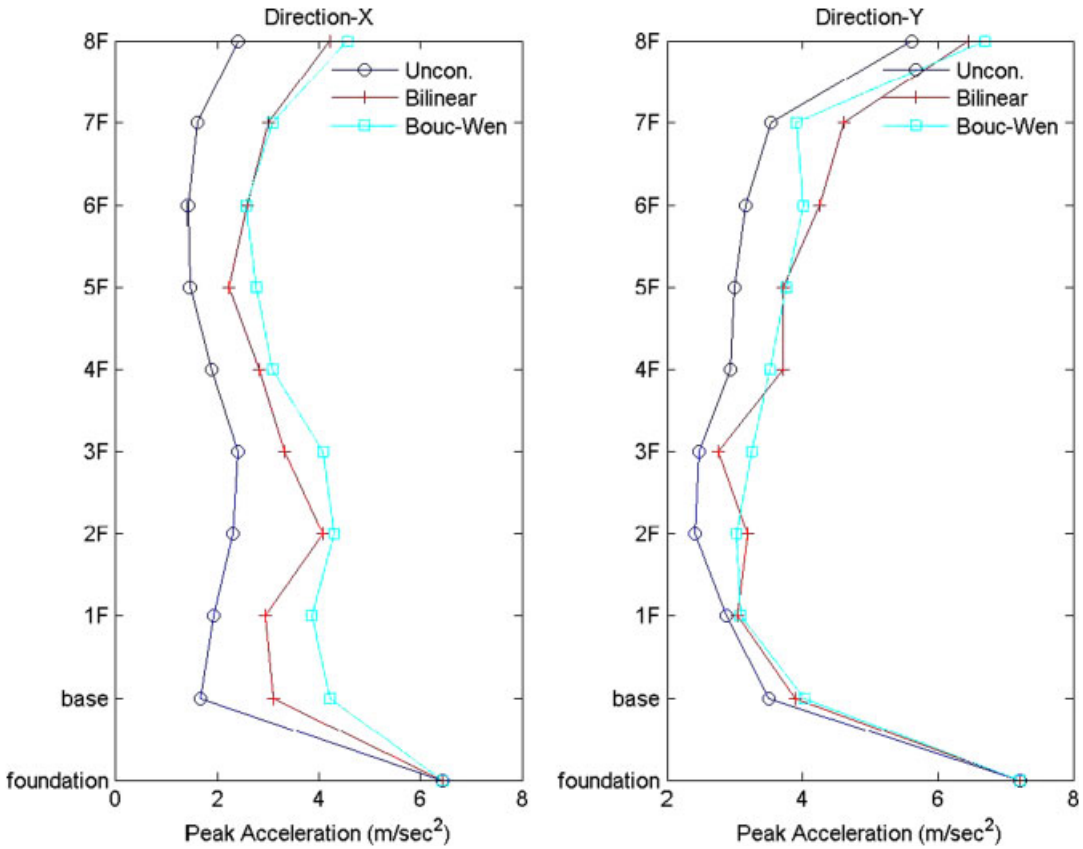

Figure 17. Responses of peak acceleration in the *x*- and *y*-direction using the MR dampers of the benchmark control problem under the excitation of the Newhall earthquake record (FP-*x* and FN-*y*).

Table III. Results of control strategies using the MR dampers provided by the benchmark control problem (FP-*x* and FN-*y*).

J_{1m}	Newhall	Sylmar	El Centro	Rinaldi	Kobe	Jiji	Erzinkan
Bilinear	0.30	1.08	−0.50	0.26	−0.68	2.12	−0.29
Bouc–Wen	0.47	0.54	0.72	0.03	−1.00	2.06	0.18
J_{2m}	Newhall	Sylmar	El Centro	Rinaldi	Kobe	Jiji	Erzinkan
Bilinear	−1.54	−1.78	−3.79	−2.60	−2.75	−0.21	−1.79
Bouc–Wen	−1.39	−2.01	−2.14	−2.52	−2.34	−0.72	−1.16

problem with better results under certain excitations. Moreover, the two control strategies also focus on the reduction of the base displacement without significantly increasing acceleration responses.

DOI: 10.1002/stc

Table IV. Results of control strategies using the MR dampers provided by the benchmark control problem (FP-y and FN-x).

J_{1m}	Newhall	Sylmar	El Centro	Rinaldi	Kobe	Jiji	Erzinkan
Bilinear	0.30	1.08	−0.50	0.26	−0.68	2.12	−0.29
Bouc–Wen	0.47	0.54	0.72	0.03	−1.00	2.06	0.18
J_{2m}	Newhall	Sylmar	El Centro	Rinaldi	Kobe	Jiji	Erzinkan
Bilinear	−1.54	−1.78	−3.79	−2.60	−2.75	−0.21	−1.79
Bouc–Wen	−1.39	−2.01	−2.14	−2.52	−2.34	−0.72	−1.16

5. CONCLUSIONS

In this study, an isolated building structure is considered to apply structural control strategies to bearing at the base. The isolation systems contain linear elastomeric bearings and nonlinear isolation bearings. Four control strategies are proposed for the semiactive case made from two different control algorithms combined with two different MR dampers. Two different types of MR dampers are selected in this study: one is provided by the sample control of this benchmark control problem and the other one is provided by NCREE and validated by the performance test at NCREE. The controller considers the output feedback control algorithm to generate the required control force. To adopt the nonlinear structural system, the control strategy has been appropriately modified into two methods: one method considers the bilinear model for the nonlinear bearings and derives four respective control gains to calculate the control force, and the other method obtains a control gain based on the initially linear system and to consider the nonlinear bearing force into the control force at the same time. All control strategies select MR dampers as control devices and simulate MR dampers based on the modified Bouc–Wen model. The inverse dynamic model of the MR dampers depends on a simplified model and clips the voltage range to drive different levels of damper force. As shown in the results, the control strategies can mitigate displacement response at the base significantly while acceleration response is slightly increased at the same time by employing the proposed MR dampers or the MR dampers of the benchmark control problem. Therefore, all of the four control strategies are effective in reducing the displacement at the base corresponding to the original goal in this study.

REFERENCES

1. Skinner RI, Robinson WH, McVerry GH. *An Introduction to Seismic Isolation*. Wiley: New York, 1993.
2. Naeim F, Kelly JM. *Design of Seismic Isolation Structures*: *From Theory and Practice*. Wiley: New York, 1999.
3. Hall JF (ed.). Northridge earthquake of January 17, 1994 reconnaissance report. *Earthquake Spectra* 1995; **11**(Suppl. C):1.
4. ICBO. Earthquake regulations for seismic-isolated structures. *International Conference of Building Officials*. *Uniform Building Code*, Whittier, CA, vol. 2, Appendix Chapter 16, 1997.
5. Asher JW, Young RP, Ewing RD. Seismic isolation design of the San Bernardino county medical center replacement project. *Journal of Structural Design of Tall Buildings* 1996; **5**:265–279.
6. Moerder DD, Calise AJ. Convergence of a numerical algorithm for calculating optimal output feedback gains. *IEEE Transactions on Automatic Control* 1985; **AC-30**(9):900–903.
7. Chung LL, Lin CC, Chu SY. Optimal direct output feedback of structural control. *Journal of Engineering Mechanics* 1993; **119**(11):2157–2173.

DOI: 10.1002/stc

8. Lu LY, Chung LL, Lin GL. A general method for semi-active feedback control of variable friction dampers. *Journal of Intelligent Material Systems and Structures* 2004; **15**:393–412.
9. Narasimhan S, Nagarajaiah S, Johnson EA, Gavin HP. Smart base-isolated benchmark building. Part I: problem definition. *Journal of Structural Control and Health Monitoring* 2006; **13**:573–588.
10. MATLAB. The Math Works, Inc., 2000.
11. Nagarajaiah S, Nagarajaiah S. Smart base isolated benchmark building. Part II: phase I sample controllers for linear isolation system. *Journal of Structural Control and Health Monitoring* 2006; **13**(2–3):589–604.
12. Erkus B, Johnson EA. Smart base-isolated benchmark building. Part III: a sample controller for bilinear isolation. *Journal of Structural Control and Health Monitoring* 2006; **13**(2–3):605–625.
13. Narasimhan S, Nagarajaiah S, Johnson EA. Smart base isolated benchmark building. Part IV: phase II sample controller for nonlinear isolation systems. *Journal of Structural Control and Health Monitoring* 2008. DOI: 10.1002/stc.267.
14. Park YJ, Wen YK, Ang AHS. Random vibration of hysteretic systems under bi-directional ground motions. *Earthquake Engineering and Structural Dynamics* 1986; **14**(4):543–557.
15. Spencer BF, Dyke SJ, Sain MK, Carlson JD. Phenomenological model of a magnetorheological damper. *Journal of Engineering Mechanics* 1997; **123**(11):230–238.
16. Loh CH, Lynch JP, Lu KC, Wang Y, Chang CM, Lin PY, Yeh TH. Experimental verification of wireless sensing and control system for structural control using MR-dampers. *Earthquake Engineering and Structural Dynamics* 2007; **36**(10):1303–1328.
17. Butcher EA, Lu R. Constant-gain linear feedback control of piecewise linear structural systems via nonlinear normal modes. *Journal of Vibration and Control* 2004; **10**:1535–1558.
18. Chang CM, Loh CH, Lu KC, Lin PY, Lynch JP. Experimental verification of wireless structural sensing and centralized/decentralized control of building using MR dampers. *Journal of Intelligent Material Systems and Structures* 2006, submitted for publication.